

COMPARING ON-ORBIT AND GROUND PERFORMANCE FOR AN S-BAND SOFTWARE-DEFINED RADIO

David Chelmins

NASA Glenn Research Center, United States of America, dchelmins@nasa.gov

Bryan Welch

NASA Glenn Research Center, United States of America, bryan.w.welch@nasa.gov

NASA's Space Communications and Navigation Testbed was installed on an external truss of the International Space Station in 2012. The testbed contains several software-defined radios (SDRs), including the Jet Propulsion Laboratory (JPL) SDR, which underwent performance testing throughout 2013 with NASA's Tracking and Data Relay Satellite System (TDRSS). On-orbit testing of the JPL SDR was conducted at S-band with the Glenn Goddard TDRSS waveform and compared against an extensive dataset collected on the ground prior to launch. This paper will focus on the development of a waveform power estimator on the ground post-launch and discuss the performance challenges associated with operating the power estimator in space.

I. INTRODUCTION

In the world of communication, software-defined radio (SDR) technology is intriguing because it provides the opportunity to develop a platform that is adaptable to unforeseen space mission needs (Ref 1). The appeal of launching a "blank slate" into space is apparent, versus hardware and corresponding functionality that was defined perhaps years before launch and will never change. One goal of communications technology is to be transparent – and therefore not limiting – to the underlying science mission (Ref 2). SDRs do not provide the ideal answer to this goal, however they do provide flexibility toward many of the constraints of traditional hardware, such as data formatting, link coding, and modulation techniques. By performing this processing in software instead of fixed hardware, the communications system exists at least partially in software and has the potential to become reprogrammable or reconfigurable.

With many of the technical challenges of SDR solved due to advent of high-speed, low-power processing hardware and wideband analog-to-digital converters (ADCs), the new challenge becomes SDR verification. That is, once a SDR is an integral part of an operational space mission, in what manner should new software or functionality be implemented to provide confidence that it will not jeopardize the mission? What assurance can an engineer on the ground provide that the in-space behavior of the new radio functionality will be as expected? On a related note, how should ground design, testing, and verification proceed when it has been shown that the in-space behavior likely will not match the laboratory performance?

In order to study questions relating to the technology development, software and hardware performance verification, and in-space operation of SDRs, NASA developed the Space Communications and Navigation

(SCaN) Testbed (Ref 3, Ref 5). NASA built and installed a payload consisting of 3 SDRs on an external truss of the International Space Station (ISS). Most of the communications testing is being performed with NASA's Tracking and Data Relay Satellite System (TDRSS) constellation of communication satellites, as well as various ground stations in the United States.

This paper will focus on the NASA Jet Propulsion Laboratory (JPL) SDR, contained within SCaN Testbed, which has an integrated S-band transceiver. The SDR hardware was developed by JPL, and the operational waveform software, the Glenn Goddard TDRSS (GGT) waveform, was developed jointly by the NASA Goddard Space Flight Center (GSFC) and the NASA Glenn Research Center (GRC). JPL also delivered test waveform software that allows evaluation of the radio hardware interfaces independent of the operational waveform.



Fig. 1: SCaN Testbed in an electromagnetic interference test chamber.

This paper will provide a background on the SCaN Testbed and the JPL SDR. The paper then will focus on the development of a received power estimator algorithm for the radio post-launch and show the differences between ground laboratory performance and observed on-orbit performance.

II. SCAN TESTBED

The SCaN Testbed (Figure 1) was developed at NASA GRC over approximately 4 years; an extensive set of ground testing was completed to verify the flight-worthiness of the payload as well as the communications performance and characteristics. SCaN Testbed was launched on the HTV-3 rocket and installed on ISS in July 2012 (Figure 2), with the first payload power-up occurring in August 2012. Shortly afterwards, the subsystem commissioning phase began where the flight computer, SDRs, and radio frequency (RF) hardware were evaluated to detect damage. Once all systems checked out, the experiments phase began and additional RF measurements were collected.



Fig. 2: SCaN Testbed installed on ISS with the Earth and a radiator in the background.

The SCaN Testbed communication paths are shown in Figure 3. The payload has both a “primary path”, used for health and status telemetry and commanding, and an “experiment path”, used for data flow between the SDRs and TDRSS. The *primary path* is the ISS mission network, which is shared with other ISS payloads and provides certain guarantees on data quality that are necessary for the safe operation of SCaN Testbed. The *experiment path* exists whenever the payload SDRs are transmitting or receiving data; in most cases, this data consists of either a pseudo-random bit sequence (PRBS) for bit error rate (BER) testing, or it can consist of non-random user data. The majority of testing to date has used PRBS data.

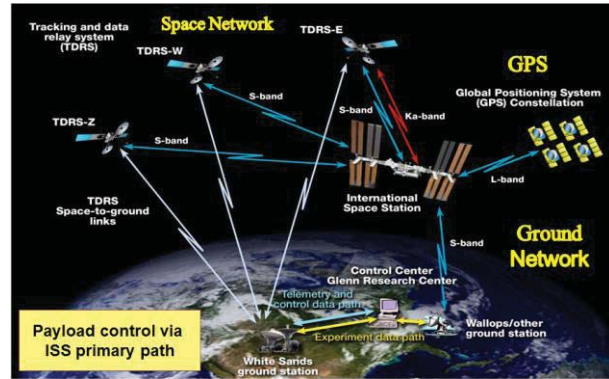


Fig. 3: SCaN Testbed communications paths, including space and ground networks.

The JPL SDR (Ref 4) is an S-band transceiver with L-band receive support. The radio size is approximately 550 in³, and it typically draws 15 W during S-band receive operations or 80 W in full duplex mode. The SDR consists of 5 slices (modules) stacked together with external interconnections: the power amplifier and power supply module, the baseband processor module, the S-band RF module, the L-band RF module, and the S-band diplexer. The ADC provides 12-bit samples with an 11 MHz bandwidth at 50 mega-samples per second (MSPS); the digital to analog converter (DAC) has a similar bandwidth and accepts 10-bit input at 50 MSPS. The baseband processing module includes a 66 MHz SPARC processor running an RTEMS operating system, as well as 2 Xilinx Virtex II field-programmable gate arrays (FPGAs) with accompanying volatile and non-volatile memory resources. Radio telemetry and control is handled by a MIL-STD-1553B interface, and data is transferred between the radio and avionics processor over a SpaceWire interface.

There are two similar JPL SDRs. The first is the flight model of the radio, which presently is located on ISS. The second is an engineering model, which is located on the ground at NASA GRC. The engineering model is similar in form, fit, and function, with the exception that some space-rated components have been replaced with commercially comparable parts.

The SCaN Testbed has RF interfaces from the three SDRs to five distinct antennas on the platform, as shown in Figure 4: one Ka-Band High Gain Antenna (HGA); one S-Band Medium Gain Antenna (MGA); two S-Band Low Gain Antennas (LGAs), one of which points towards the Earth and is denoted as the Near-Earth Network-LGA (NEN-LGA), while the other points towards space and is denoted as the Space Network LGA (SN-LGA); and finally one L-Band GPS LGA that solely interfaces with the JPL SDR. Both the Ka-Band HGA and S-Band MGA are gimballed antennas which are controlled via an interface between Avionics and the Gimbal Control Electronics unit. The

three S-Band antennas are interchangeably available to the payload SDRs via an RF switch network.

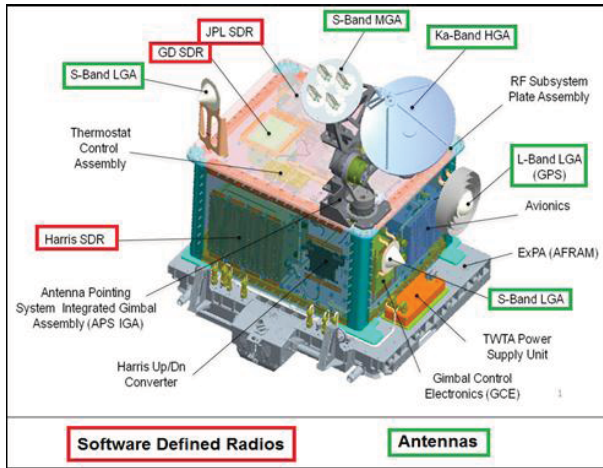


Fig. 4: SCaN Testbed SDRs and antennas. The RF signal routing is contained within the payload and allows the radios to communicate through any of the relevant antennas.

III. GROUND TESTING

The JPL SDR (Figure 5), along with the other radios in SCaN Testbed, underwent a significant ground test period during which RF testing was conducted in a controlled environment. In addition to steady-state tests of the forward (receive) and return (transmit) links of the radio, thermal vacuum testing was conducted to evaluate radio performance over temperature.



Fig. 5: JPL SDR flight model. The engineering model is identical in appearance and has similar functionality.

Ground testing mostly was conducted with the GGT waveform operating on the JPL SDR platform, which led to some ambiguity between platform performance and waveform performance. In itself, this is not a significant problem provided the flight system is tested using the same waveform. However, this creates an issue for future waveform development, since the

performance measured on the ground then is tied to a particular implementation of SDR software.

Forward link testing focused on determining the radio and waveform response to an incoming signal in terms of telemetry and communication link performance metrics such as BER. Curves were produced showing the relationship between BER and a given energy per bit to noise density ratio (E_b/N_0). Data was collected on the performance effect of interferers injected at various power levels and frequency offsets.

Return link testing similarly focused on determining the expected performance of a ground radio, primarily one similar to that used for TDRSS support. The power amplifier characteristics were measured and calibrated to reduce spurious emissions and maximize linear power output. Ground radio performance was characterized using a TDRSS Simulator provided by Real-Time Logic, Inc., which resulted in BER curves over a variety of E_b/N_0 ratios.

IV. GGT RECEIVED POWER ESTIMATOR DESIGN

The GGT waveform was designed for the purpose of evaluating the space-to-space link BER performance, however it soon was adapted to support user data. One of the first improvements after launch of the SDR was implementing a received power telemetry item to show the receiver signal strength. This value provides insight into the expected link bit BER performance, which cannot be measured directly for a channel of user data.

The received power is estimated using a narrow-band filter near the center of the receiver bandwidth. The filter assumes that the radio receive frequency is tuned properly, so the measured power out of the filter will contain the signal main lobe power plus some low level of noise.

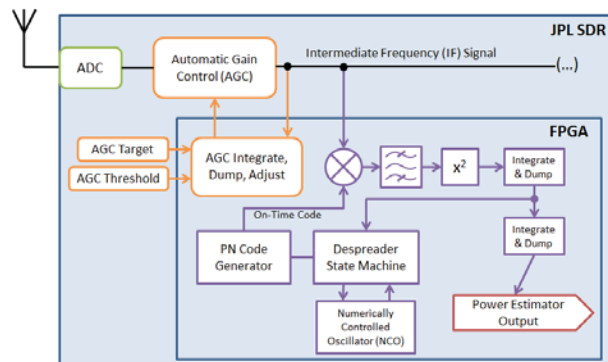


Fig. 6: GGT power estimator. The estimation is provided by leveraging the despreader on-time filter.

The power estimator, which is a part of the waveform despreader, is shown as a block diagram in Figure 6. The input to the despreader is the down-converted intermediate frequency signal, which should

be accurate in frequency to approximately 1 kHz due to the SDR temperature compensated crystal oscillator (TCXO) stability. The despreader uses the well-known early, on-time, and late replica technique with a locally-generated pseudo-noise (PN) code, and the replicas are mixed with the incoming signal to generate early, on-time, and late correlations. These correlations are passed through bandpass filters on each channel (early, on-time, late) to allow the in-band signal power to be extracted and determine the fractional frequency to adjust the numerically controlled oscillator (NCO) of the local PN code to maximize the on-time signal power. The bandpass filters are implemented digitally, which allows the passband bandwidth to change according to the expected main lobe bandwidth of the signal (typically twice the data rate in Hz) plus an allowance for Doppler.

The received power estimate is determined by averaging the signal power in the on-time filter via an integrate-and-dump operation. For a spread signal, the despreader will keep the on-time power maximized. For a non-spread signal, the despreader has no effect and is bypassed in the receiver; however, its digital filters still can be used to estimate power as long as the incoming signal is not mixed with any local PN replicas.

V. POWER ESTIMATOR IMPLEMENTATION, CALIBRATION, AND TESTING

The power estimator was developed and verified on the ground using the SDR engineering model. One hypothesis of SCaN Testbed is that a waveform (or waveform component) can be developed on the ground and expected to have comparable performance in space. The set of ground testing conducted using the flight radio prior to launch must be sufficient to allow future development and performance prediction. The power estimator was the first evaluation of this concept on the JPL SDR.

The original GGT waveform tested on the ground included a despreader, so adding the power estimator involved averaging the on-time filter output and determining the calibration between the resulting engineering value and the actual input power level. The averaging is implemented in the FPGA (refer to Figure 6), while the calibration is applied in the general purpose processor (GPP) portion of the waveform.

In order to calibrate the power estimator, a test was conducted where the radio input signal power was swept from -50 dBm to -122 dBm in 1 dB increments. The power was held at each increment until a sufficient amount of samples could be taken to update the power estimator averaging filter. Once a valid measurement was made, the engineering value was recorded along with the measured radio input power. The calibration process was repeated for the 10 variations (referred to as “modes” – shown in Table 1) of symbol rate, frequency, and spreading contained within the GGT waveform. In this paper, only power levels up to -100 dBm will be considered since that is the highest power that is observed while communicating with TDRSS. Also, this is convenient because the effects of the AGC algorithm can be ignored. As the input power increases, the AGC reduces amplification, which causes the despreader to effectively see less signal power. Fortunately, the AGC is relatively constant for power levels under -100 dBm because noise power saturates the adjustment loop. Similarly, -120 dBm is a reasonable lower bound for the spread modes (A, B, C, D) since the waveform is unable to maintain carrier lock below this level. Modes E and F lose lock around -116 dBm, while modes G and H lose lock around -106 dBm.

and spreading contained within the GGT waveform. In this paper, only power levels up to -100 dBm will be considered since that is the highest power that is observed while communicating with TDRSS. Also, this is convenient because the effects of the AGC algorithm can be ignored. As the input power increases, the AGC reduces amplification, which causes the despreader to effectively see less signal power. Fortunately, the AGC is relatively constant for power levels under -100 dBm because noise power saturates the adjustment loop. Similarly, -120 dBm is a reasonable lower bound for the spread modes (A, B, C, D) since the waveform is unable to maintain carrier lock below this level. Modes E and F lose lock around -116 dBm, while modes G and H lose lock around -106 dBm.

MODE	SPREAD	SYMBOL RATE (KSPS)	FREQ. (MHZ)	FILTER BW (KHZ)
A	Yes	18	2106	149
B	Yes	36	2106	188
C	Yes	18	2041	149
D	Yes	36	2041	188
E	No	155	2041	450
F	No	310	2041	789
G	No	769	2041	1793
H	No	1538	2041	3468

Table 1: GGT Waveform Modes of Operation. The spread column indicates whether the waveform mode uses PN spreading. The symbol rate is the transmitted symbols per second. The frequency is the center frequency of the mode. The filter bandwidth is the 3 dB cutoff of the despreader bandpass filter used for making the power measurement.

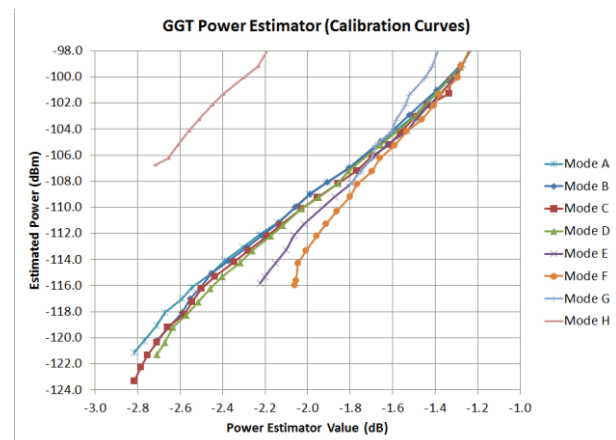


Fig. 7: Power estimator ground calibration curves collected on the JPL SDR engineering model.

The different modes of operation produce distinct calibration curves between the measured filter power value and the actual input power, shown in Figure 7.

Each mode is considered separately when generating a curve fit to map estimator values into received power, however many of the curves have similar shape. The spread spectrum modes (A, B, C, and D) have similar calibration curve characteristics and are consistent except for very low power levels. Around -120 dBm, the signal is so small that the noise power begins to influence the measurement. Ideally, the power estimator bandwidth would be reduced to make a better measurement, however, because this is on the fringe of the operating range, it was simpler to adjust the calibration curves to a polynomial fit. The non-spread modes (E, F, G, H) all have higher symbol rates and therefore higher bandwidth. The power estimator values are also slightly larger than the spread modes for a given power because of the additional noise integrated into the signal. Mode H has a reduced AGC target to improve waveform data performance (unrelated to the power estimator). Unfortunately this target significantly increases the AGC's response to the noise floor and the impact on the estimated power value, so the results will be poor for Mode H.

Once calibration curves were determined for the 10 modes, the equations were loaded into the GGT waveform and a code release was generated for the flight system.

VI. ON-ORBIT TESTING CONSIDERATIONS

The ground-based testing provided data points in performance on 1dB increments over a very large range in input power, which is the ideal approach to characterizing the waveform. Unfortunately, this is not possible when using the TDRSS system as the RF source with nominal pointing methodologies. As the ISS is in a Low Earth Orbit, while TDRSS is in a Geosynchronous Orbit, the two platforms are not in constant line of sight. For the most part, the SCaN Testbed can see TDRSS via one of the gimballed antennas for a maximum of 40 minutes, based upon the limitations of the gimballed range of motion (Figure 8).

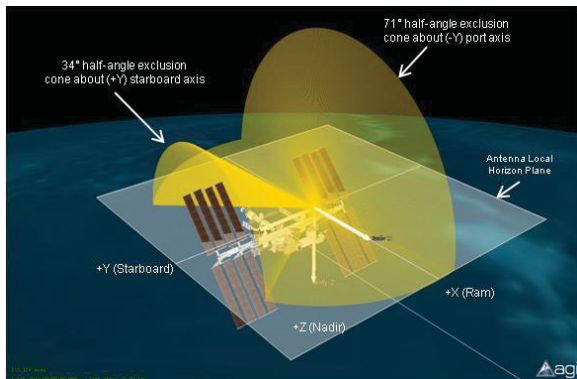


Fig. 8: SCaN Testbed Gimbal Space

The gimballed S-Band MGA is required for this testing. While using the S-Band MGA, the gain variation over the link should be ideally zero, as the antenna is actively pointed towards the TDRSS RF source. Path loss variations from these two types of orbital platforms provide roughly 2dB of input power variation, assuming that the link covers the full 40 minute possible contact window. TDRSS provides two power level modes of operation, thus a waveform can only be tested at two 2dB input power bands, which are not adjacent or overlapping. This provides a distinct gap in the testing methodology between ground-based testing and nominal on-orbit testing.

However, as the gimballed antennas are moved by the Antenna Pointing System (APS) via pre-defined motion profiles, those profiles are not required to be nominally pointed. GRC has developed the methodology to purposefully off-point the antenna such that the received power to the SDR can be pre-defined via experimenter requirements (Ref 6). The S-Band MGA provides the experimenter with roughly 28dB of receive gain variation, over its main lobe, which has a first antenna null at 47° off boresight, as shown in the on-orbit antenna pattern in Figure 9.

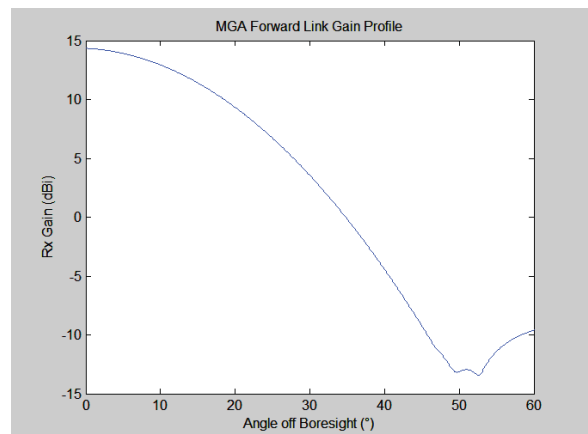


Fig. 9: S-Band MGA On-Orbit Antenna Pattern

While the paper in (Ref 6) describes the methodology where power levels are held and changed in more linear approaches, it is not the only methodology that has been derived. Using the spiral search algorithm that is part of the Ka-Band tracking function of the APS, thresholds are set to a high value such that spiral motion is an on-going process. For Ka-Band tracking, there is also a threshold for which the system would transition to autotrack functionality, but for this set of tests, the autotrack capability can also be fully disabled so that it is never triggered. Figure 10 illustrates the continual spiral motion during an HGA characterization test, for the purpose of illustrating the type of motion capable via this methodology.

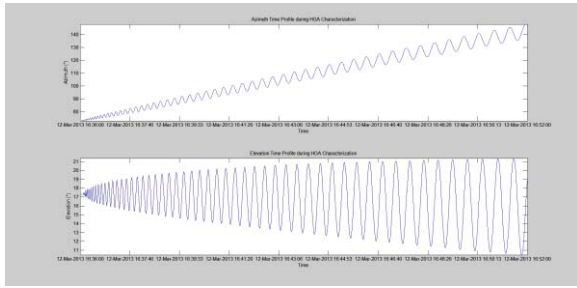


Fig. 10: Nominal pointing with embedded spiral motion.

For this characterization testing, the embedded spiral search methodology was used over the nominal pointing, in conjunction with an extra pre-defined pointing error. This methodology allows for the received power level to be constantly varying, which allows for more instances to be examined for waveform response. The pre-defined error was defined as the error necessary for the minimum received power to be obtained while using the nominal 1° spiral lap size. This error varies with the duration of each scheduled event. Offsets were defined in the gimbal elevation axis, since this axis is generally unchanged by staleness of the ISS ephemeris. To induce a change in the elevation axis, the ISS would need to perform an orbital maneuver which changes the orbital plane's ascending node, as opposed to nominal burns to boost altitude, which induce errors in the argument of periapsis. Nominal predictions of the RF performance is performed in the SCA Testbed Analysis Tool (STAT) software tool, and antenna off-pointing profiles are created to target the desired range of received power. STAT is a project-generated tool that contains the RF characterized data of the TDRSS spacecraft, as well as for SCA Testbed. Access times and RF predictions are generated via STAT, and can be viewed for future events or past events, via archived orbital Two-Line Element (TLE) data files for ISS and TDRSS spacecraft. STAT is illustrated in Figure 11.

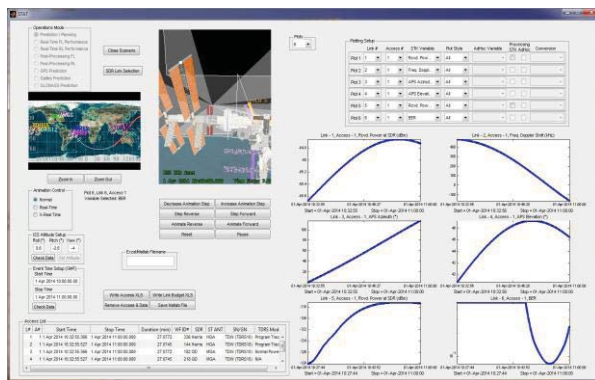


Fig. 11: STAT Overview Screen

VII. ON-ORBIT TESTING RESULTS

The on-orbit test was conducted in all modes using a spiral motion and collecting power estimator values at a rate of 1 value every 5 seconds. The on-orbit results for the spread spectrum modes of operation are shown in Figures 12 through 15. The results for non-spread modes of operation are shown in Figures 16 through 19. The X-axis of the curves has been held constant, although the Y-axis changes since some of the waveform modes have smaller operating power ranges. Also, the on-orbit received power is limited for certain modes (such as A and B) due to the available transmit power of TDRSS. In these figures, the solid blue line is the calibration curve shown earlier (Figure 8), and the various markers on the charts are the actual data points obtained during on-orbit testing using the MGA antenna sweep procedure. The tests are labelled in an YYYY-DD/T format, where YYYY is the year, DD is the Julian day of year, and T is the sequential RF test number conducted by SCA Testbed on that day. The individual data points are not as important as the overall trend and distribution of data points across many trials.

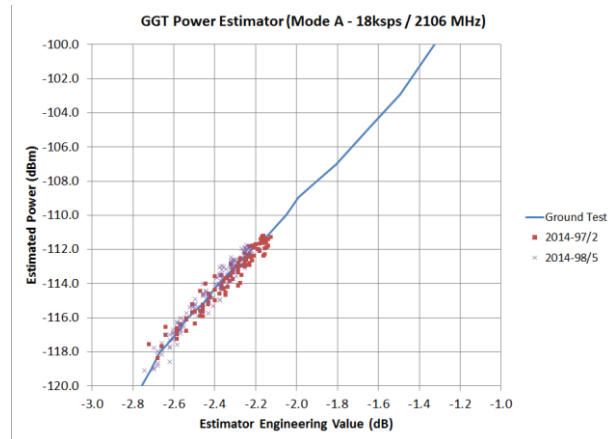


Fig. 12: Results for GGT mode A.

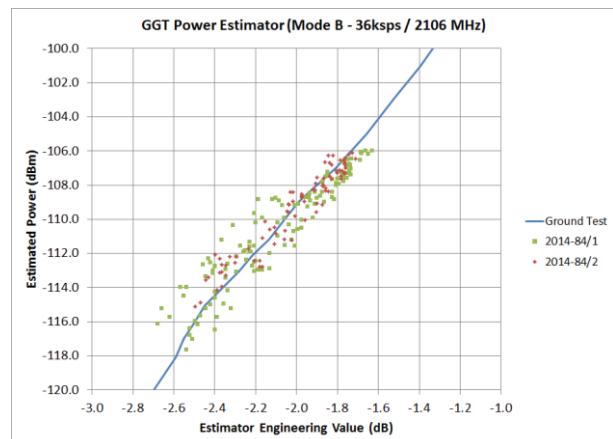


Fig. 13: Results for GGT mode B.

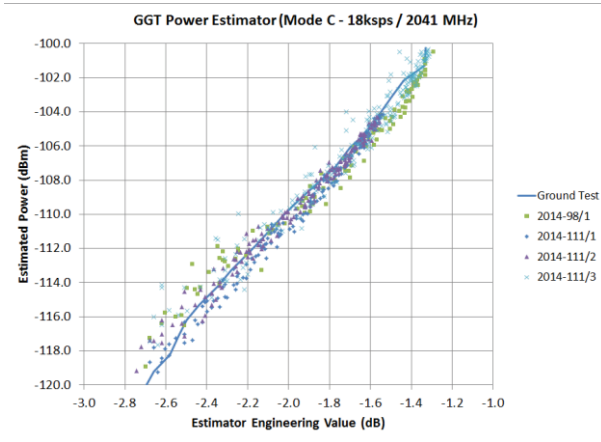


Fig. 14: Results for GGT mode C.

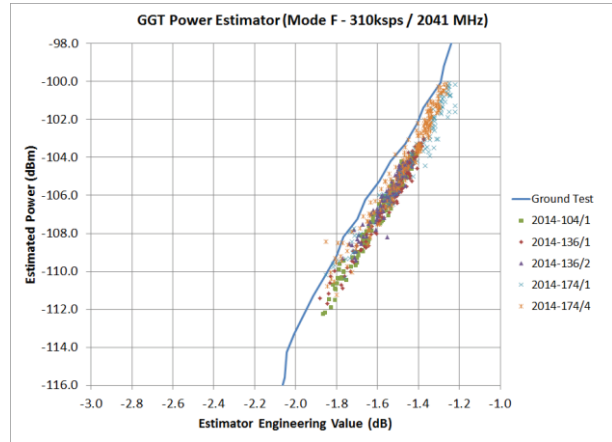


Fig. 17: Results for GGT mode F.

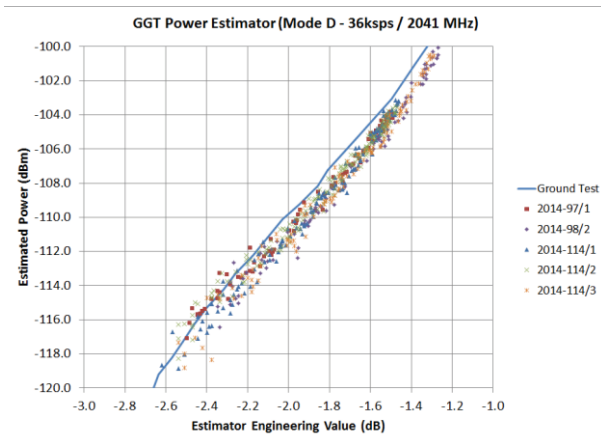


Fig. 15: Results for GGT mode D.

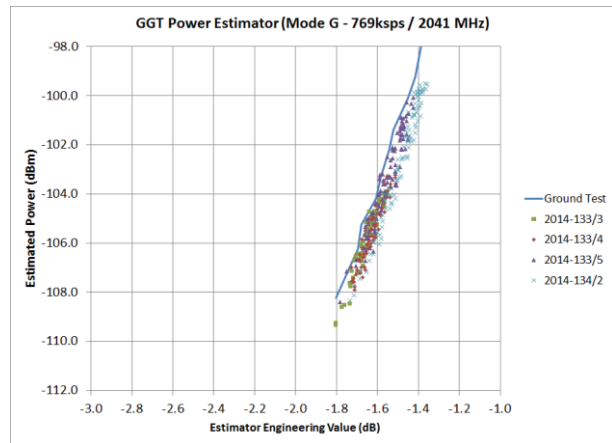


Fig. 18: Results for GGT mode G.

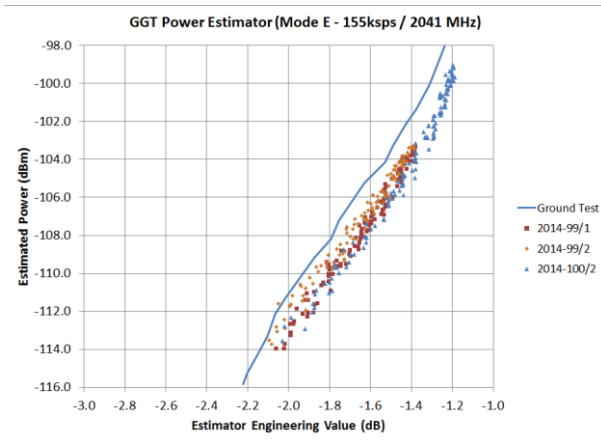


Fig. 16: Results for GGT mode E.

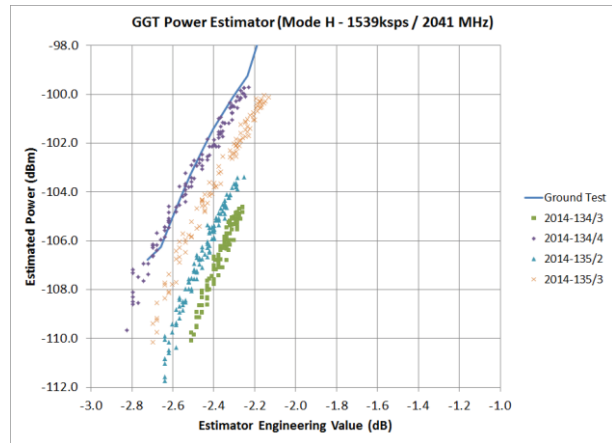


Fig. 19: Results for GGT mode H.

The summary of the above results, in terms of the average offset of the on-orbit measurements and the standard deviation of the offset, is provided in Table 2.

MODE	AVERAGE ERROR (DB)
A	0.1
B	0.3
C	0.6
D	0.8
E	2.2
F	1.5
G	0.4
H	10.9

Table 2: Average estimator error (offset)

The results are interesting because they show that, without modifying any parameters from the ground calibration, the estimator is reasonably accurate for spread modes (A, B, C, D) but has worse performance for non-spread modes (E, F, G, H). The spread modes show less than 1 dB of error in most cases. The non-spread modes E and F are slightly worse, with under 2 dB of error. Mode G is excellent, with under 0.5 dB error, which indicates that the ground calibration matched the space environment well. As expected, Mode H has poor performance due to the lowered AGC set point and the effect that will have on the downstream signal level. In all cases, the estimator indicates a power that is higher than what is actually being received on-orbit.

Since the estimator actually provides signal plus noise power, the noise floor difference between the engineering model and flight model was considered. When applied over the filter bandwidth, the error for the spread modes is reduced by 0.1 dB and the error for modes E, F, G, and H is reduced by 0.2, 0.3, 0.5, and 0.9 dB, respectively. Accounting for the noise power provides an improvement to the estimator error, but it is not a significant change.

The AGC is another potential source of error. The AGC is an uncontrolled variable in these tests, and it is sensitive to wideband noise since it takes a power measurement over the entire IF bandwidth. While the noise floor can be understood in a laboratory environment, it is not possible to maintain the same level of consistency for a space test. The spread modes take up a large bandwidth (approximately 3 MHz) versus the non-spread modes, so the AGC mainly considers signal power when setting the gain level. On the other hand, the non-spread modes have significantly smaller bandwidth requirements, so the AGC mainly considers noise/interferer power when setting the gain level. This results in varying power levels on the intermediate frequency signal, which violates the power

estimator assumption that the AGC is relatively steady below -100 dBm.

Also, the incoming noise and interference power is difficult to estimate because it depends on many factors: antenna angle, payload spatial position, time, ISS radiator/array positions, etc. Interference effects are less noticeable in the spread modes (A, B, C, D) because the PN spreading results in signal gain while reducing interferer level. Due to the spreading gain, the power estimator will be more accurate for spread modes since it considers the “on time” replica inside the despreader.

VIII. CONCLUSIONS AND FUTURE WORK

This paper presented a simple power estimator that is based on an integrate-and-dump operation covering the expected signal bandwidth. The power estimator utilizes a digital filter within the waveform despreader to make its power estimate; for spread waveforms the “on time” replica is used, and for non-spread waveforms the filter is simply applied to the IF bandwidth.

The results show that this approach provides reasonable results (less than 1 dB error) for PN spread waveform modes. The PN signal bandwidth and spreading gain appear to deliver a more consistent result that is less sensitive to noise and interference. The approach provides worse results (1 to 2 dB error) for non-spread signals, and very poor results (10 dB error) for signals that require significant AGC adjustments.

The power estimator presented in this paper is suitable for implementation with low-rate spread spectrum waveforms. The implementation was successful even with all code development being completed on the ground using a radio engineering model; the code was then installed on the space radio without prior testing of the space radio in a controlled environment.

Future work is needed to develop a better model for the AGC. Variable levels of interference and noise are a significant consideration for space operations, and the AGC algorithm must be either very stable or well-understood in order to compensate for noise effects on the power estimator. Additionally, more investigation is needed to see whether narrowing the bandpass filter bandwidth will yield a more accurate result as the received signal power decreases.

IX. REFERENCES

- [1] “Software Defined Radios | NASA”, http://www.nasa.gov/directorates/heo/scan/engineering/technology/txt_sdr.html, retrieved August 4, 2014.
- [2] “Space Technology Roadmaps – Communications and Navigation Systems”, TA05, <http://www.nasa.gov/offices/oct/home/roadmaps/>, retrieved August 4, 2014.
- [3] “SCaN Testbed”, <http://spaceflight systems.grc.nasa.gov/SOPO/SCO/SCaNTestbed/>, retrieved August 4, 2014.
- [4] J. Lux, “Software Defined Radios (SDR) for NASA Spaceflight Applications”. <http://hdl.handle.net/2014/43463>, retrieved August 5, 2014.
- [5] S. K. Johnson, R. C. Reinhart, and T. J. Kacpura, “CoNNeCT’s approach for the development of three software defined radios for space application,” in Proc. IEEE Aerospace Conference, 2012, pp. 1–13.
- [6] B. W. Welch, M. T. Piasecki, M. W. Shalkhauser, and J. C. Briones, “On-Orbit Characterization of SDRs on ISS Utilizing Antenna Off-Pointing Capabilities on the SCaN Testbed,” Antenna Measurement & Techniques Association 2014.